

Research Article

In Vitro Model of Neurotrauma Using the Chick Embryo to Test Regenerative Bioimplantation

Aina Mogas Barcons¹, Divya M. Chari² and Christopher F. Adams³

¹Sheffield Institute for Translational Neuroscience, University of Sheffield, Sheffield, UK; ²School of Medicine, Neural Tissue Engineering Group, Keele University, Newcastle-under-Lyme, UK; ³School of Life Sciences, Neural Tissue Engineering Group, Keele University, Newcastle-under-Lyme, UK

Abstract

Effective repair of spinal cord injury sites remains a major clinical challenge. One promising strategy is the implantation of multifunctional bioscaffolds to enhance nerve fibre growth, guide regenerating tissue and modulate scarring/inflammation processes. Given their multifunctional nature, such implants require testing in models which replicate the complex neuropathological responses of spinal injury sites. This is often achieved using live, adult animal models of spinal injury. However, these have substantial drawbacks for developmental testing, including the requirement for large numbers of animals, costly infrastructure, high levels of expertise and complex ethical processes. As an alternative, we show that organotypic spinal cord slices can be derived from the E14 chick embryo and cultured with high viability for at least 24 days, with major neural cell types detected. A transecting injury could be reproducibly introduced into the slices and characteristic neuropathological responses similar to those in adult spinal cord injury observed at the lesion margin. This included aligned astrocyte morphologies and upregulation of glial fibrillary acidic protein in astrocytes, microglial infiltration into the injury cavity and limited nerve fibre outgrowth. Bioimplantation of a clinical grade scaffold biomaterial was able to modulate these responses, disrupting the astrocyte barrier, enhancing nerve fibre growth and supporting immune cell invasion. Chick embryos are inexpensive and simple, requiring facile methods to generate the neurotrauma model. Our data show the chick embryo spinal cord slice system could be a replacement spinal injury model for laboratories developing new tissue engineering solutions.

1 Introduction

There is a global drive to develop therapies which can safely and effectively restore function of the injured spinal cord. Given the complexity of spinal cord injury (SCI), the major challenge is to develop combinatorial therapies which can achieve multiple clinical goals (e.g., promoting and directing regeneration of nerve fibres, modulation of immune responses, degradation of inhibitory scar tissue). Bioscaffolds offer a chemical and physical environment to support neural cell growth. They can be made from natural polymers to mimic native tissue extracellular matrix or synthetic polymers with linked agonists to improve neural tissue growth. In addition, modified bioscaffolds can secrete molecules to promote regeneration or be loaded with transplant cell populations for replacing damaged tissue (Doblado et al., 2021; Boni et al., 2018; Führmann et al., 2017).

A key requirement in developing therapeutic bioscaffolds is the ability to evaluate multiple biomedical readouts in relevant, neuromimetic injury models. Currently, bioscaffolds are tested in isolated cell cultures with progression to live animal models of spinal injury. Such cell cultures are unlikely to provide multifaceted, physiologically relevant data as they lack multiple cell types, 3D cytoarchitecture and cell-cell interactions of native tissue. Live adult animal models also have considerable drawbacks for testing and optimising bioscaffold formulations. For example, they are technically complex and time consuming, expensive, due to animal numbers required to generate statistically significant data and are associated with substantial ethical implications in introducing long-term spinal injury.

Organotypic slices of rodent spinal cord tissue have been proposed as an ‘intermediate stage’ between cell culture and adult animal experimentation in order to screen promising materials in neurorepresentative environments. In culture, these slices maintain *in vivo* cell types and cytoarchitecture. Further, a transecting injury can be introduced, and the tissue displays typical pathological responses to the injury such as glial scarring, immune cell infiltration and limited nerve fibre outgrowth. Using this system, Weightman et al. (2014), demonstrated that aligned electrospun scaffolds implanted into injured rodent spinal cord slices were able to direct regeneration, highlighting the model’s utility. More recently, Walsh et al. (2023) used transverse mouse spinal cord slices cultured on hydrogels to demonstrate a translationally relevant, 3D printed GelMA hydrogel did not cause adverse astrocyte and microglia reaction when interfaced with nervous tissue. However,

Received April 17, 2023; Accepted October 20, 2023;
Epub November 2, 2023; © The Authors, 2023.

ALTEX 41(#), ###-###. doi:10.14573/altex.2304171

Correspondence: Christopher Adams, PhD
School of Life Sciences, Neural Tissue Engineering Group,
Keele University, Newcastle-under-Lyme, ST5 5BG, UK
(c.adams@keele.ac.uk)

Advantages of the chick embryo versus rodent in vitro model of spinal injury



	
Possesses all major spinal cord cell types and spinal cord structure	
Protected species – partial replacement of animal experimentation	Not protected under Directive EU/2010/63 before E15 – replacement strategy
Requires dedicated infrastructure	Requires 37°C incubator
Needs animal handling expertise	Facile techniques
Litters are genetically similar	Egg batches genetically diverse
ca. £8.00/rodent	ca. £0.80/egg

Fig. 1: Schematic summarizing advantages of using the chick embryo to derive organotypic slice models of spinal cord injury versus rodents

overwhelmingly tissue is currently derived from rodents which have high maintenance costs, requiring housing facilities, dedicated care personnel and food. In addition, slices are generally derived from one litter, limiting genetic variability within biological repeats. Further, if embryonic rodent tissue is required, the mother also has to be sacrificed to access the tissue, adding ethical considerations.

As an alternative to rodent derived tissue, the chick embryo is a well-defined model of the mammalian nervous system extensively employed in neurodevelopmental research (Himmels et al., 2017). In terms of the spinal cord, all major central nervous system cell types are established by embryonic days 9-10 (E9-10). Further, vascularisation and neuroarchitecture, such as cortico-spinal tracts, are also observed at this time (Ferretti and Whalley, 2008). Before E15, the chick embryo spinal cord is considered ‘regeneration permissive’ and displays nerve outgrowth and neural progenitor proliferation in response to transection injury. Further, chicks with spinal cords transected before E15 are able to operate their lower limbs at hatching. Post E15, transections to the chick spinal cord have impaired regeneration and the chicks show a lack of function of the lower limbs at hatching (Hasan et al., 1993; Shimizu et al., 1990; Whalley et al., 2006). In addition, microglia are present in the developing cord from E3 (Calderó et al., 2009). Microglia are nervous system immune cells and key mediators of inflammatory tissue responses to biomaterials. Use of the chick embryo may also contribute to the drive to reduce, refine and replace animal use (the 3Rs) within the neural tissue engineering field. Prior to E15 the chick embryo is not protected under Directive EU/2010/63 and is not considered a protected species according to the Animals (Scientific procedures) Act of 1986 (UK), so could be used as a replacement strategy for animal experiments. Moreover, due to its development *in ovo*, the embryo can be accessed without harming the mother and a batch of eggs usually comes from more than one hen, improving genetic diversity in comparison to rodents. Further, chick embryo culture is cost-effective as eggs are also significantly cheaper than rodents (ca. £0.80 versus £8 each) and require limited infrastructure and expertise in handling, so protocols could be adopted by regenerative neurology laboratories worldwide (Figure 1).

Elegant studies have previously demonstrated successful organotypic culture of chick embryo spinal cord slices (Tubby et al., 2013; Yang et al., 2019). Whilst important, these were focussed on aspects of spinal cord development and were not investigating responses to injury. Further, the models employed transverse slices not able to recapitulate nerve fibre tract regeneration, were cultured for short periods of time (up to 7 days) and did not investigate glial cells roles, all of which are important when considering modelling traumatic injury. Despite its potential, the utility of the chick embryo has never been assessed for generating slice models of SCI within which new tissue engineering strategies can be tested.

In this study we aimed to assess (i) The feasibility of establishing organotypic spinal cord slices from chick embryo tissue (ii) The neuropathological responses to a transecting injury in organotypic spinal cord slices from chick embryo tissue and (iii) the feasibility of implanting a bioscaffold and the subsequent regenerative response in the injury.

2 Methods

2.1 Ethics

Given the aim of the experiment is to test biomaterial modulation of neuropathological responses, we wanted to ensure all relevant cell types were present with established cytoarchitecture in place so we chose the latest time-point the embryo is considered to be non-protected (E14). We subsequently received approval to sacrifice the embryos under Schedule 1 procedures from the local Animal Welfare and Ethical Review Body. Sacrifice was by decapitation, in accordance with approved methods of sacrifice for vertebrate embryos Animals (Scientific Procedures) Act 1986.

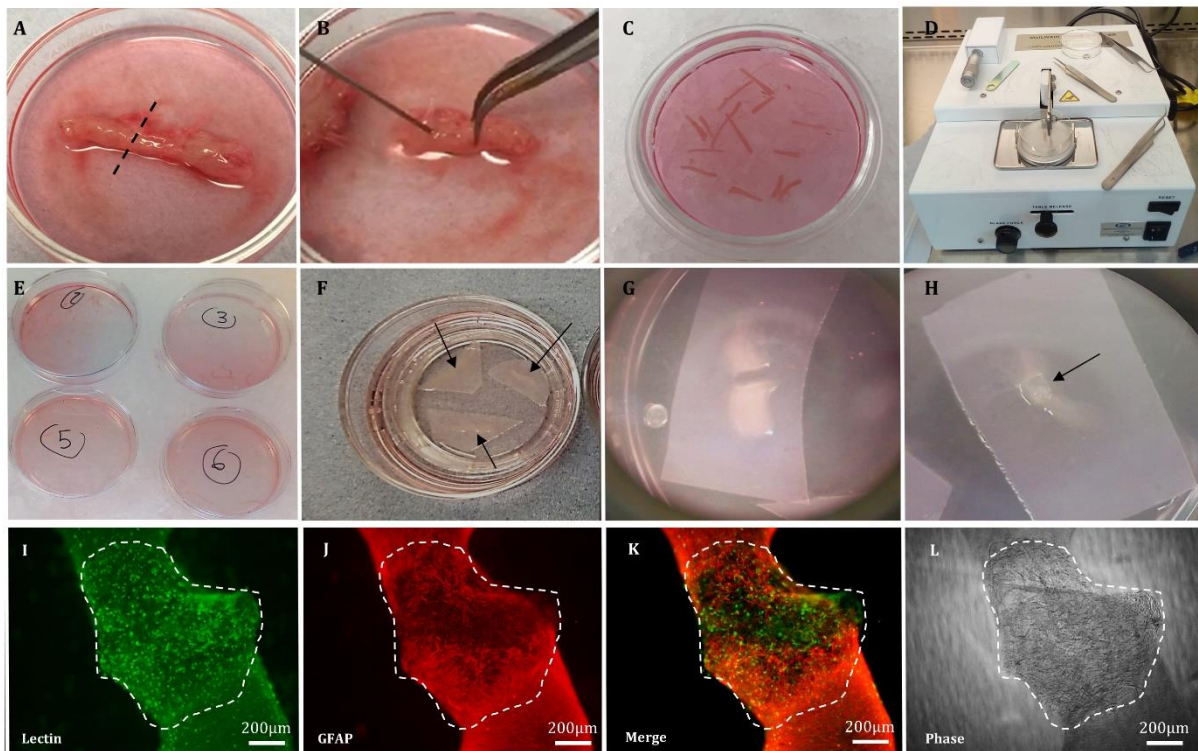


Fig. 2: Images depicting experimental overview

The spinal column was dissected (A) and the spinal cord ejected using a stream of slicing medium (B). Multiple cords were collected in one Petri dish (C) before slicing using the Mcllwain tissue chopper (D). Slices were then added to Petri dishes (E) containing pre-cut membranes (F). A transecting injury was introduced into the slice (G) and in some slices biomaterial implantation was performed (H). (I-L) Representative fluorescent and phase images showing bioimplant integration with the injured spinal cord slice tissue. Dashed line indicates outline of implant. Cellular infiltration is noted within the implant (I-K), the fibres of which can be seen under phase microscopy (L).

2.2 Experiment overview and time-points

Spinal cords were dissected from E14 chick embryos, sliced longitudinally and cultured. These slices were injured at two different time points: 4 days post dissection (I4) and 12 days post dissection (I12). Each of these groups were split and fixed at a further two different time points: 4 days post injury (denoted I4F4 and I12F4) or 12 days post injury (denoted I4F12 and I12F12). The viability of each of these time points was controlled with an uninjured spinal cord slice that was fixed at the same time. These timepoints were required to investigate the effects of an early vs. late injury and whether the response to injury changed over time. For bioimplantation experiments, slices were injured at 4 days and immediately implanted with the scaffold. These slices were then cultured to the maximum time point from previous experiments, 20 days post-injury/implantation (24 days total culture). The overall experimental scheme is shown in Figure 2, which shows spinal cord extraction, spinal cord slicing, spinal cord culture and injury and finally biomaterial implantation into the injury site. Biomaterial implantation showed good integration with injured tissue, determined as cellular infiltration into the bioimplant at the lesion margins, as shown in Figure 2I-L. These steps are described in more detail in the rest of the methods.

2.3 Establishing organotypic slices from chick embryo spinal cords

Fertilized Bovans Brown eggs (Henry Stewart & Co.) were incubated at 37°C and 47% humidity in a specialised egg incubator (Brinsea) (Incubation parameters were chosen as indicated by Brinsea). After 14 days, the embryos were extracted, sacrificed and a 1.5 - 2 cm section of the spinal column was dissected out. The spinal cord was ejected by a stream of slicing medium [HEPES (2.5%; BioSera L0180-100), EBSS (97.5%; Invitrogen 24010-043)] injected through the spinal canal. All spinal cords were kept in slicing medium on ice until use (up to a maximum of 1 h).

The spinal cord slice organotypic culture and lesioning protocols were adapted from Weightman et al. (2014). Here, each spinal cord was sliced longitudinally at 350 µm thickness with a Mcllwain Tissue Chopper, collected in a small petri dish containing ice-cold slicing medium and kept on ice for 30 minutes. Around 3 intact slices could be generated from each spinal cord. Meanwhile, the culture chambers were prepared. A permeable insert (Millicell, PICMORG50) was placed in a small petri dish and three 0.45 µm pore, 0.5 cm² size membranes (Omnipore JHWP04700) were placed on top of the insert. The insert provides a raised platform so slices can be cultured at an air:medium interface. The space between the petri dish and the insert was filled with 1.1 mL of culturing medium (MEM (Invitrogen 42360-024), horse serum (25%; BioSera S0910-500), EBSS (19%), glucose (5%), pen-strep (1%; Fisher 11528876). After 30 minutes, the spinal cords were collected with a wide-bore transfer pipette and placed on the membranes (one spinal cord slice/membrane). These membranes have previously been used for successful rodent spinal cord slice culture (Weightman et al., 2014) and facilitate manipulation of one spinal cord at a time e.g. for transfer to a well for individual staining. Finally, the small petri dishes were placed on a large square petri dish for easier transportation and for better sterile protection and kept inside an incubator at 5% CO₂ and 37°C. The slices were fed

every other day by 50% medium change until fixation at the required time point (all steps shown in Figure 2A-H). For fixing, slices were washed in PBS once, incubated in 4% PFA for 1h at room temperature, washed three times with PBS then kept at 4°C for further staining.

2.4 Introduction of a transecting lesion in the organotypic spinal cord slices and implantation of Hemopatch™

Transecting lesions were induced in sterile conditions under a dissection microscope. A double-blade scalpel was used to mark the lesion edges to ensure equal injury size in all slices. Then, the spinal cords were completely sectioned with a standard scalpel aided with a needle following the marks of the double-bladed scalpel. The slice debris between the two injury margins was removed with tweezers. For the implantation experiments, a 250 µm thick slice of uncoated and acellular Hemopatch™ (Hemopatch™ was kindly donated by Baxter Healthcare Technologies) was implanted into the lesion. Hemopatch™ is a clinical grade bovine collagen scaffold used as a sealant in neurosurgical procedures. We have previously shown its utility for supporting neural transplant populations (Mogas Barcons et al., 2021), highlighting potential for repair mediating implantation in sites of neurological injury. To achieve implantation, under sterile conditions, a 0.5 cm² piece of Hemopatch™ was cut with a scalpel and then chopped with a McIlwain Tissue Chopper set to 250 µm. These pieces were then placed adjacent to the slice and further cut to the size of the lesion with a scalpel. Then, it was implanted to bridge the gap between two sides of the lesion (Figure 2I-L). Finally, the slices were kept in the incubator and fed with culturing medium (50% change) every 2-3 days for 20 days until they were transferred into 24-well plates for fixation.

2.5 Immunostaining

After fixing, spinal cord organotypic slices were washed 3 times for 5 minutes in PBS and then incubated with blocking solution [PBS + 0.3% Triton X-100 (Sigma T9284) + 10% Normal Donkey Serum (Jackson ImmunoResearch 017-000-121)] for 30 min at RT. Then, the samples were incubated at 4°C overnight with the appropriate primary antibody or biotinylated lectin suspended in blocking solution. Primary antibodies were anti-Tuj-1 for nerve fibres and neurons (1:500; Biolegend; 802001), anti-GFAP for astrocytes (1:500; Biolegend; 644702), anti-MBP for myelin and oligodendrocytes (1:200; BioRad; 160223). The next day, the samples were washed and incubated with the appropriate secondary antibodies in combination with DAPI (4',6-diamidino-2-phenylindole) (5.0 µg/mL) in blocking solution for 2 h at RT in the dark and then washed 3 times, 5min/wash. Secondary antibodies were Cy-3 or FITC tagged IgG antibodies (or anti-biotin for lectin detection) all from Stratech and used at 1:200. Finally, the samples were mounted on glass slides with Vectashield mounting medium (Vector H-1000) and covered with a glass coverslip.

2.6 Live/dead assay

30 minutes prior to fixing, some samples were incubated with 6 µM Ethidium homodimer (Sigma E1903), 4 µM of Calcein-AM (VWR 89139-470) and 5 µg/mL of DAPI in DMEM, incubated for 20 minutes in 5% CO₂ at 37°C, washed with PBS, mounted on glass slides and imaged live.

2.7 Imaging

Images of spinal cord organotypic slices were taken under a fluorescence microscope (Leica DMC 2500 LED) equipped with a CCD camera (DFC350 FX) unless stated otherwise. The software used for imaging was Leica Application Suite X v.1 (2017). All spinal cord slice images were taken at consistent light exposure parameters throughout the experiments.

2.8 Quantification and statistical analysis of organotypic spinal cord slices

2.8.1 Slice health

Images of stained spinal cords taken at 5x magnification were used for this analysis. First, the images for each channel (red and green for Ethidium homodimer staining and Calcein AM staining respectively) were converted to 8-bit. Then, the optical density (OD) background value was obtained for each channel as the mean OD of 5 different areas of the image outside the spinal cord. Then, the mean OD value of the full image for each channel was obtained and corrected by subtracting the background. The corrected values were added to obtain a total fluorescence value and, finally, a viability index was obtained as the percentage of corrected viable OD relative to the total OD value. The survival data for transection experiments was analysed with a two-way ANOVA and Tukey correction. The survival data for the implantation experiments, was analysed with a Kruskal-Wallis test with Dunn's correction.

2.8.2 GFAP expression

5x images of GFAP stained spinal cords were converted to 8-bit. Using imageJ, a vertical line, perpendicular to the injury margin, was drawn from the lesion margin towards the centre of the slice and the OD profile of the line was generated. The average OD was then calculated at three regions: 0-10 µm, 50-60µm and 100-110µm. The process was repeated three times for each slice to obtain an overall slice average at each region. Then, the background was calculated by averaging the mean OD value of three different regions outside the slice in each image, which was subtracted from the previously averaged slice OD values to obtain a corrected OD value for each region of each spinal cord. A repeated measures two-way ANOVA with Sidak's multiple comparison test was used to statistically analyse the data.

2.8.3 Axonal infiltration into the lesion

For injury alone experiments, the total number of axons infiltrating the lesion was analysed. 20x magnification consecutive images of the whole width of the lesion were fused together in a panoramic image using Microsoft PowerPoint 2016 and

opened in ImageJ. All axons that were sprouting from the lesion margin were counted and divided by the full width of the slice (mm). However, this protocol was not usable after biomaterial implantation due to the intricate web of axonal infiltration within the material meaning it was difficult to accurately count single axons. Therefore, the total length of all infiltrated axons in the lesion was calculated and compared between unimplanted and implanted slices. Here, three 40x images were taken at random areas within the lesion and uploaded to the NeuronJ plugin in ImageJ. The axons were traced and the total length of traced axons in μm was obtained. The results from the three fields were averaged to generate an axonal length measurement for each slice. A Kruskal-Wallis test with Dunn's correction was performed for statistical analysis.

2.8.4 Lectin expression

Lectin quantification was achieved by counting the number of lectin-positive cells that were detached from the spinal cord slice per unit area (mm^2) at the lesion site using a standard size grid overlaid onto each image. Three images were obtained for each slice and the total number of lectin positive cells per area was averaged. The results were statistically analysed with a Kruskal-Wallis test with Dunn's correction.

2.8.5 Statistical analysis

All statistical analysis was performed, and graphs plotted using GraphPad Prism 9 (version 9.5.1). Data are presented as mean \pm standard error of the mean (SEM) unless otherwise stated. Experimental 'n' number is reported where each 'n' is one separate slice.

3 Results

3.1 Organotypic spinal cords could be derived from the chick with lesioning producing characteristic neuropathological responses

Initial experiments showed all major neural cell types, astrocytes, neurons, oligodendrocytes, and microglia, could be detected within the cultured chick embryo spinal cords (Figure 3). Nerve fibre networks staining positive for Tuj-1, were observed in all slices. These fibres displayed both random orientation and occasional stereotypical aligned orientation (Figure 3A). MBP staining was observed in all slices and in general appeared as fibrous in nature (Figure 3B). MBP staining was often coincident with nerve fibre staining, following the nerve fibre patterns (Figure 3C). In around 20% of slices, tracts of myelin staining were observed running longitudinally along the spinal cord slice (Figure 3D). A dense network of GFAP positive astrocytes was detected in all slices (Figure 3E). Finally, lectin staining was detected (Figure 3F). However, in our hands, lectin staining was capricious and required multiple attempts at staining to achieve sufficient data for quantification purposes. When successful, lectin positive microglia could be observed at regular intervals throughout the spinal cord tissue and displayed a ramified morphology, associated with an exploratory (non-inflammatory) phenotype (Figure 3F).

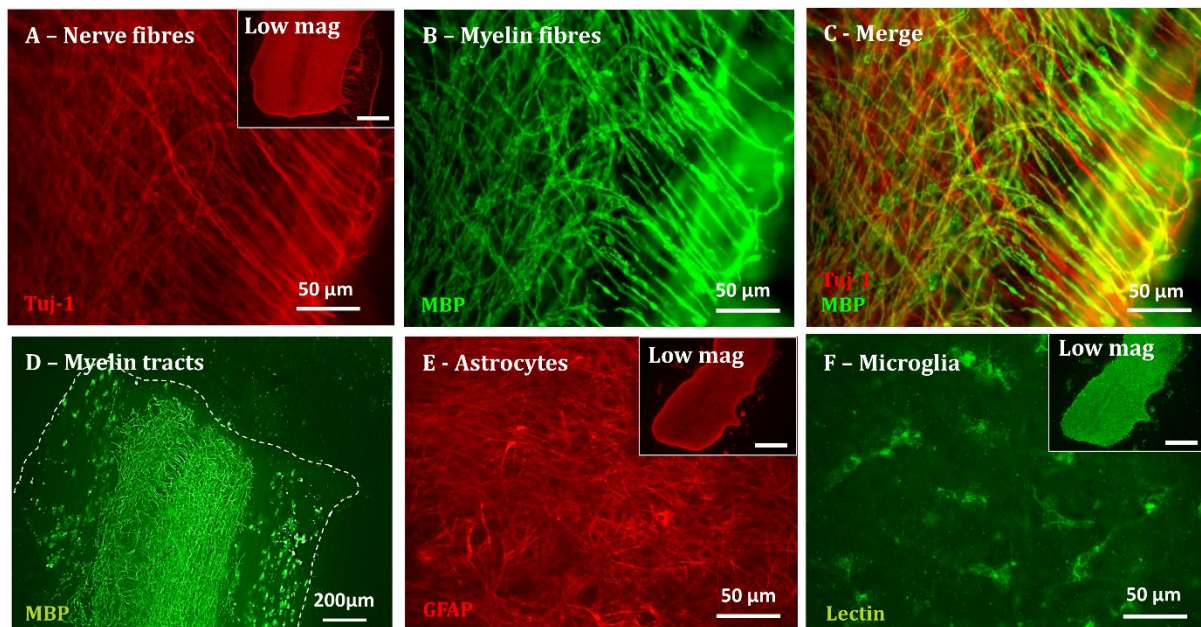


Fig. 3: Representative fluorescent images showing neural cell staining in chick embryo spinal cord slices

(A) Representative image of Tuj-1 positive nerve fibres; (A-inset) representative low magnification image of Tuj-1 stained slice. (B) Counterpart image to (A) depicting MBP positive fibres, appearing to follow similar patterns to the nerve fibres; (C) merge of A and B. (D) Low magnification image showing myelin tracts, which were observed in around 20% of slices. Dashed line depicts slice edges. (E) Representative image of GFAP staining with dense network of GFAP fibres/astrocytes; (E-inset) representative low magnification image of GFAP stained slice. (F) Representative image of lectin positive microglia which were distributed throughout the tissue and mostly adopted a ramified morphology; (F-inset) representative low magnification image of lectin stained slice. Scale bars in insets are 500 μm .

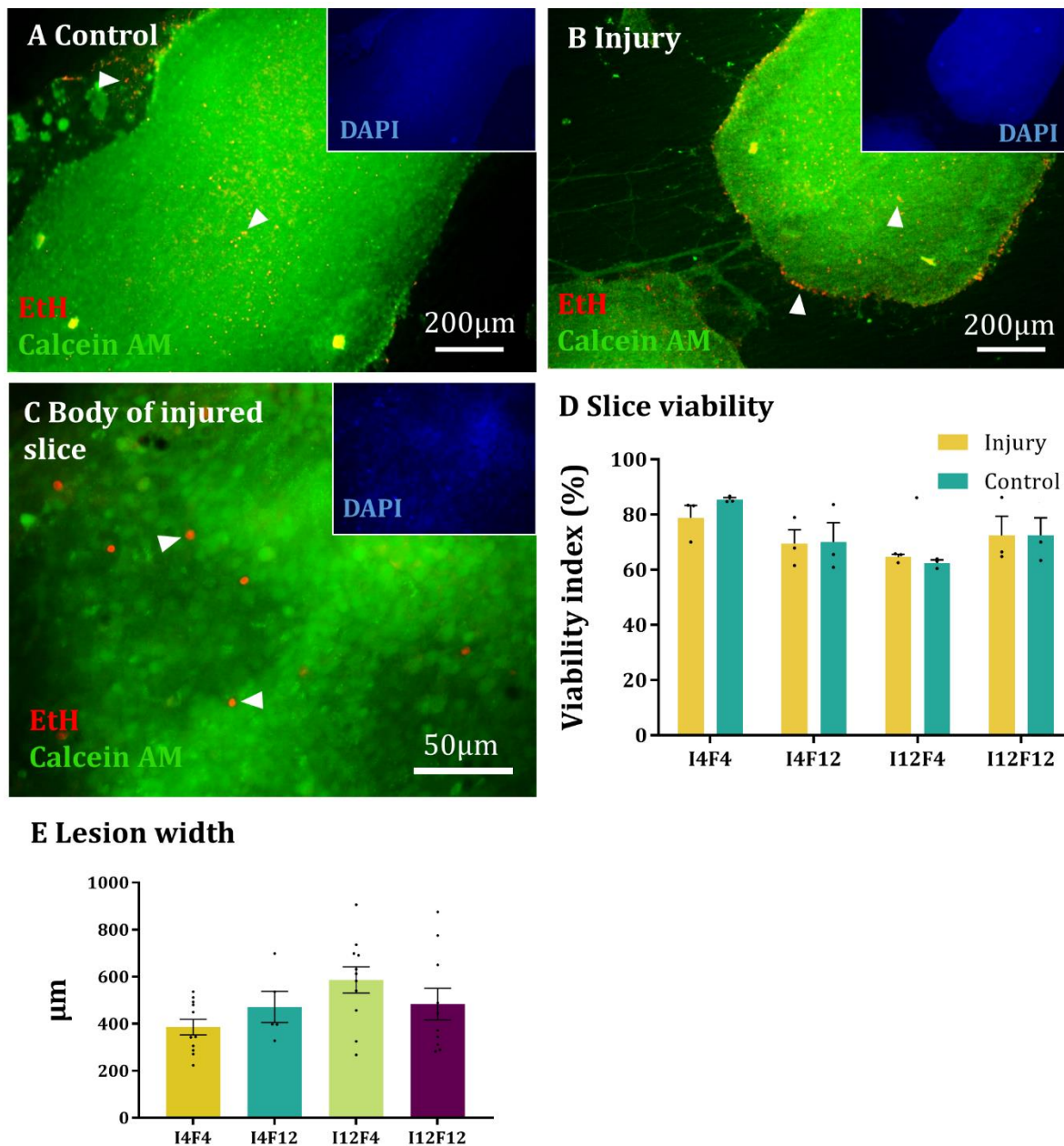


Fig. 4: Slices retain high viability and the lesion width is consistent over time

(A-C) Representative double-merged fluorescent images showing live (green), dead (red) and DAPI (inset) staining of control (A) and injured (B) organotypic slices. Arrowheads indicate dead cells. The injury in (B) is in the bottom left of the image. (C) shows a high magnification field of an injured slice, where a limited number of dead cells can be observed (arrowheads). (D) Bar chart showing quantification of live staining compared to dead staining, represented as a viability index. No statistical differences were found across all experimental conditions (Two-way ANOVA, $p > 0.05$, $n = 3$). (E) Bar chart showing quantification of lesion width at each experimental time-point. No statistical differences in lesion width were detected across conditions (One-way ANOVA, $p > 0.05$, $n = 10$).

Within lesioning experiments, all spinal cords showed calcein-AM staining, an indicator of cellular health, throughout the tissue, regardless of whether they had been lesioned or not (Figure 4A, B). At high magnification it was possible to see single dead cells spread across the spinal cord (Figure 4C), which were mostly accumulated outside the edges of the slice or at injury margins. Approximately, between 60 and 80% of the spinal cord was stained with calcein-AM. There were no statistically significant differences in overall slice viability between injured and uninjured slices or between time points (Figure 4D). At each time-point, lesion widths appeared to be consistent in size and after quantification there were no statistical differences in lesion width between groups, with an average width ranging from ca. 400 to 500 µm (Figure 4E).

During microscopic observation it was noted that the lesion margins of spinal cords were stained more intensely with anti-GFAP than the centre of the spinal cord (Figure 5A-D). Further, at the lesion margin, GFAP positive cell morphologies were characterised by elongated somas and processes, distributed in parallel to each other and perpendicular to the lesion (Figure 5E), in contrast with the random network distal from the lesion (Figure 5E inset). Microglia, detected as lectin-positive

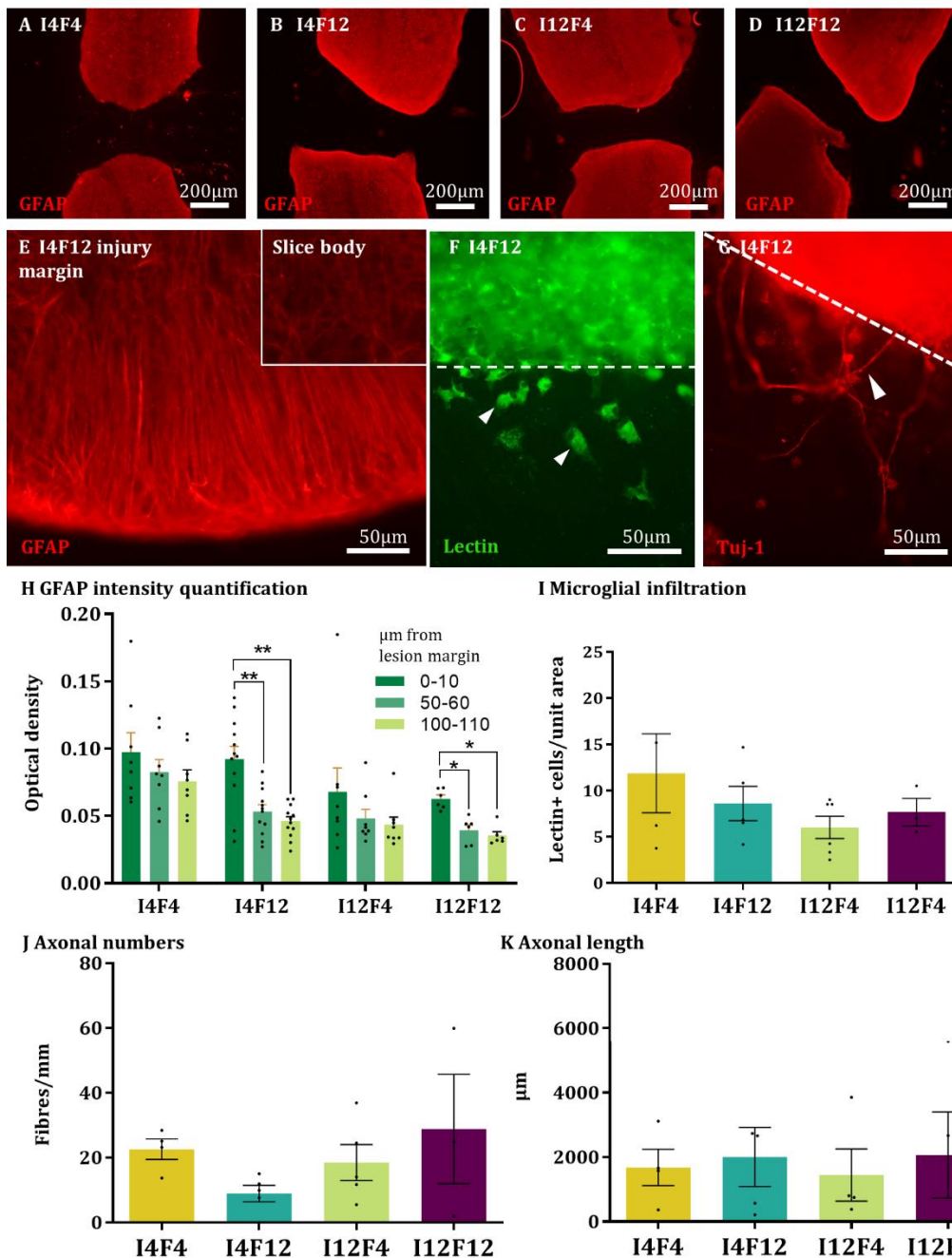


Fig. 5: Classical neuropathological responses are detected after traumatic injury in chick embryo spinal cord slices
 (A-D) Representative fluorescent images showing GFAP staining of spinal cord slices when injured at four days in vitro and cultured for four (A) or 12 (B) days more or when injured after 12 days in vitro and cultured for four days (C) or 12 (D) days more. (E) Representative high-magnification fluorescent image depicting GFAP staining at the injury margin and in the slice body (inset). Note the aligned morphology of the astrocytes at the lesion margin, perpendicular to the injury. (F) Representative fluorescent image showing microglia infiltration into the injury site. (G) Representative image depicting TuJ-1 stained nerve fibres projecting into the injury. (H-K) Bar charts showing quantification of (H) GFAP intensity at different distances (0-10, 50-60 and 100-110 μm) away from the injury margin, (I) numbers of microglia infiltrating the injury site, (J) numbers of nerve fibres per mm projecting into the injury and (K) average length of projecting nerve fibres. Statistical differences in (H) are highlighted as * $p < 0.05$ and ** $p < 0.01$ (Two-way ANOVA, $n = 5 - 12$). No statistical differences were found in I-K (One-way ANOVA, $n = 5 - 12$).

cells, were seen infiltrating the lesion gap. The cells infiltrating the lesion presented an amoeboid morphology while cells visualised within the centre of the slice appeared more ramified (Figure 5F). TuJ-1 staining showed limited axonal sprouting into the lesion gap. The nerve fibres extended in a haphazard fashion with no particular direction favoured and were never observed to reconnect both sides of the lesioned spinal cord (Figure 5G). OD analyses revealed a significantly higher GFAP expression between 0-10 μm from the lesion margin than at 50-60 μm and 100-110 μm from the lesion margin for the spinal cords that were fixed 12 days post injury. This higher GFAP expression was not seen for those that were fixed at 4 days post injury (Figure 5H). The number of infiltrating microglia cells per unit area was similar in all time points (Figure 5I).

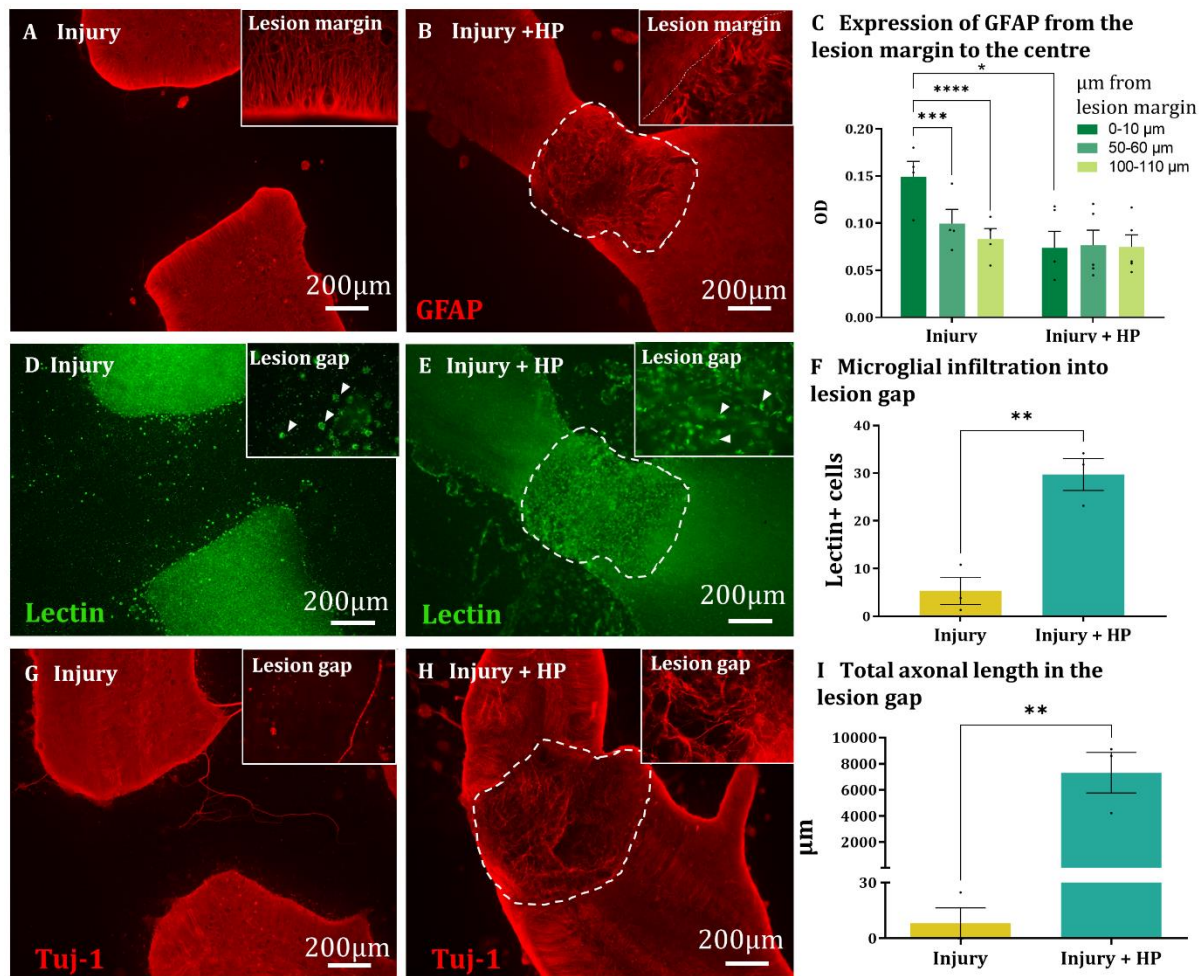


Fig. 6: Bioimplantation modulates neuropathological responses at the injury site in injured chick embryo spinal cord slices

All images are from 24 days in culture where slices were injured after 4 days and then cultured for a further 20 days. (A, B) Representative fluorescent images showing GFAP staining in (A) control, unimplanted slices and (B) slices with Hemopatch™ implanted into the injury. (A, B insets) High magnification images of GFAP staining at the injury margin in each condition. (C) Bar chart indicating quantification of GFAP expression at different distances from the lesion margin. (D, E) Representative fluorescent images showing lectin staining of microglia in (D) control, unimplanted slices and (E) slices with Hemopatch™ implanted into the injury. Note, A and D are counterpart images from the same experimental slice and B and E are also counterpart fluorescent images from the same experimental slice. (D, E insets) High magnification images of lectin stained cells within the injury in each condition. (F) Bar chart indicating quantification of numbers of microglia in the injury site. (G, H) Representative fluorescent images showing Tuj-1 staining of neurons and nerve fibres in (G) control, unimplanted slices and (H) slices with Hemopatch™ implanted into the injury. (G, H insets) High magnification images of Tuj-1 staining within the injury in each condition. (I) Bar chart indicating quantification of total axonal length per field within the injury site. In (C) statistical differences are highlighted as, *** $p < 0.001$ (Two-way ANOVA, $n = 4 - 5$). In (F) and (I) statistical differences are ** $p < 0.01$ (unpaired t-test, $n = 3$). HP – Hemopatch™.

Approximately 20 axonal fibres were counted per mm from one side of the lesion with a relatively high variation amongst slices (between 20 and 60 fibres/mm) within the same time point (Figure 5J). The total length of sprouting axons per field was also highly variable (from 0 to 6000µm), with no statistical differences between time points (Figure 5K).

3.2 Bioimplantation modulates neuropathological responses in injured chick embryo spinal cord slices

In order to examine whether biomaterials could be implanted into the injury site and potentially modulate regenerative responses, slices were injured as above, and half were implanted with Hemopatch™ with half remaining as controls (non-implanted). Similarly, to the previous experiments, the spinal cords in the control group had a higher expression of GFAP at the edge of the lesion, with the cells apparently aligned at 90° to the lesion (Figure 6A, C). However, when Hemopatch™ was implanted, GFAP expression was not higher at the lesion edge than at the centre of the spinal cord and the orientation of GFAP positive cells seemed random at all distances from the lesion (Figure 6B, C). A visual assessment of the treated spinal cord slices indicates that infiltrating GFAP-positive cells expressed more GFAP than those within the tissue. However, their morphology and cytoarchitecture differ from untreated slices as seen by the loss of polarity towards the lesion and the lack of a clear band of orientated astrocytes, expressing high levels of GFAP (Figures 6A, B). Biomaterial implantation induced high microglial infiltration into the implanted biomaterial compared to infiltration within the lesioned area alone. Visual analysis of the lectin-positive cells morphology suggested most of the infiltrated cells to present an amoeboid or reactive phenotype

(Figure 6D-F). In terms of nerve fibres, implantation of HemopatchTM, resulted in robust axonal infiltration within the material with high numbers of nerve fibres detected in the lesion area, which were absent in controls (Figure 6G, H). The total axonal length in each microscopic field was 10,000-fold higher in implanted versus control injury sites (Figure 6I).

4 Discussion

Here we show for the first time that longitudinal 3D slices of chick embryo spinal cord tissue can be derived and cultured for extended periods of time (at least 24 days), in the lab. Major neural cell types are present with classical cytoarchitecture observed (nerve fibre tracts, myelin tracts and interwoven astrocytes). Further we showed that neuropathological responses to transecting injury commonly associated with adult injury could be observed, that were modified with bioimplantation of a clinical grade scaffold material. Chick embryos are simple to maintain and cost-effective. Therefore, the data show this model could have substantial impact in enhancing accessibility to high-validity neurological injury models, for a range of laboratories. This includes neuroscience laboratories with little or no infrastructure for animal experimentation, or to facilitate cross-disciplinary research with material engineering laboratories.

When considering neuropathological response, our data on GFAP expression post-injury are in line with previous rodent studies. For example, we only saw an increase in GFAP expression at the lesion margin compare to the slice body at 12 days post injury but not at four days. Although highly variable in the literature, visible changes in GFAP expression are generally reported to occur several days after the injury (Bradbury & Burnside, 2019). In comparable experiments, Weightman et al. (2014) report GFAP upregulation at the injury margin at seven days post injury in rodent organotypic slice models of spinal cord injury. We also report that GFAP OD at the edge of the lesion was lower after biomaterial implantation than in injured, non-implanted slices. Moreover, astrocytes, which were polarised in a 90° angle in respect to the untreated lesion, appeared more disperse and less elongated on the implanted slices, suggesting a possible disruption of glial reactivity. These results are supported by studies which report a disruption of the glial scar either through an architectural change in vivo (Hurtado et al., 2011) or a decrease in GFAP expression in vitro (Guijarro-Belmar et al., 2019; Weightman et al., 2014). Therefore, even though there is a slower change in astrocyte reaction to the injury, the effects of bioimplantation on astrocyte regenerative responses can be assessed within the chick embryo model. Some studies demonstrate no difference in glial scar formation after biomaterial implantation (Domínguez-Bajo et al., 2020; Galli et al., 2018). Varied data across the literature could be due to the use of different types of biomaterials (i.e.: aligned fibres, injectable hydrogels, implantable gels), stressing the importance of biomaterial screening tests before committing to higher complexity, live animal models.

We also report high axonal infiltration within the implanted biomaterial compared to the untreated lesion, similar to previously published research in vivo (Galli et al., 2018; Wu et al., 2018; Yang et al., 2015) and in vitro (Guijarro-Belmar et al., 2019; Weightman et al., 2014). We were unable to distinguish any possible physical reconnection between axons from each end of the lesion. Nevertheless, the high number of infiltrating axons is suggestive of a potential pro-regenerative role for axonal growth (or regeneration permissive role) of HemopatchTM implantation. An exciting further development could be to fuse the model with specialist multielectrode array systems capable of recording electrophysiological activity at multiple points across the whole spinal cord slice. These could measure recovery of spinal cord network activity across the lesion after injury and any therapeutic manipulation.

As far as we are aware, this is the first report of immune cell infiltration in an implant in the chick. Our data indicate that microglial infiltration in the lesion area is higher upon implantation. Moreover, morphological examination seemed to indicate that microglia displayed a reactive phenotype within the biomaterial. Our results are in consonance with previously published research with mouse organotypic models of transecting SCI (Weightman et al., 2014) and in vivo models of transecting SCI in rats and mice respectively (Domínguez-Bajo et al., 2020; Kourgiantaki et al., 2020). A reduction in microglial infiltration has only been reported in one study (Guijarro-Belmar et al., 2019), due to the functionalisation of the implanted biomaterial with an Epac2 agonist. However, there were some technical issues with lectin staining, including high background and inconsistent staining success. Lectins can be less specific than antibodies and may highlight different features from microglia such as blood vessels (Sharma et al., 2022). Future work should aim to employ chick specific microglial antibodies such as anti-chick CD45 (Calderó et al., 2009), which we could not source at the time of this study.

Establishing the slice model still requires sacrifice of the embryo. However, this can be performed at a stage where the animal is not-considered protected (before third trimester) and before the embryo would be able to survive outside of the egg on its own (before E16). Further, as opposed to embryonic rodent models, there is no requirement to sacrifice the mother. The use of embryonic tissue does mean direct inference to adult nervous system injury cannot be made. Further, vascularisation and the blood brain barrier (BBB; important components to injury and regeneration pathology) are absent in the chick embryo slice model. To address these issues, ageing the slices through extended culture may allow for “older” tissue neuropathological responses to be assessed. Organotypic slices of neural tissue have been cultured for several weeks, indicating this is a possible strategy. Introduction of a BBB would be challenging. However, in terms of tissue engineering, implants are designed to come in direct contact with nervous tissue to elicit the mechanism of action. We have shown that nervous tissue responses can be observed using the chick embryo slice model, indicating the model has utility in investigating these specific mechanisms of action. Whilst the model will not be able to completely replace live adult animal models of SCI, it may offer a replacement with reduced ethical implications for research at early stages of therapy development. It must be noted though that, as scientific opinion on embryo sentience is constantly changing, ongoing review is required with relation to the method of embryo sacrifice.

There may be species specific differences in neuropathological responses to injury/bioimplantation between chicks and humans and chicks and rodents. Therefore, some caution is needed when interpreting the data. Other approaches offer a means to address some of these issues. Researchers are developing organoid models of the spinal cord using human induced pluripotent stem cells (hiPSCs; Lee et al., 2022; Xue et al., 2022), which overcome species specific differences. However, it

is still difficult to mimic the cytoarchitecture of the spinal cord using organoids, especially longitudinal tracts. Further, common protocols for organoid development are extended (e.g., at least 6 weeks) and longer-term culture poses issues of necrosis in the hypoxic organoid centre. In terms of bioimplantation, organoids may also pose a technical challenge in biomaterial interfacing given their small size (ca. 1-3 mm in diameter). In general, hiPSC derived cultures also lack the neural immune cells, a major component of the tissue reaction to biomaterials. Alternatively, there is also a possibility of introducing human cells into tissue slices through xenografting. A recent study by Ogaki et al., (2022) demonstrated the replacement of microglia in rodent organotypic slices with human hiPSC derived microglia, which could be tested within the chick embryo slice model.

Some materials used in the culture and analysis of the chick embryo spinal cords are derived from animals (e.g. horse serum, antibodies). Establishing the model using non-animal derived materials is an important next step. Serum has been shown to be crucial for maintaining CNS architecture in tissue slices (Yang et al., 2019), so may be challenging to replace. However, there are several commercial serum alternatives that could be tested. There is also a drive towards using chemically defined medium for in vitro cell and tissue culture, so a chemically defined medium for chick embryo slice culture could be attempted. In terms of analytical procedures, more antibodies are now being synthesised using recombinant cell lines, so should be examined as replacements for any animal derived antibodies. Further, classical histological dyes could be used to detect nerve fibres (e.g., silver staining), myelin (luxol fast blue) and overall tissue changes (H&E staining). These may offer an alternative, animal free route to analyse tissue changes after injury and biomaterial implantation.

In conclusion, we have been able to show that using a simple, cost-effective tissue model based on the chick embryo, researchers can potentially establish a model of high utility for testing new regenerative therapies for spinal cord injury.

References

- Boni, R., Ali, A., Shavandi, A. et al. (2018). Current and novel polymeric biomaterials for neural tissue engineering. *Journal of Biomedical Science*, 25, 90. doi:10.1186/s12929-018-0491-8
- Bradbury, E. J., & Burnside, E. R. (2019). Moving beyond the glial scar for spinal cord repair. *Nature Communications* 10, 1–15. doi:10.1038/s41467-019-11707-7
- Calderó, J., Brunet, N., Ciutat, D. et al. (2009). Development of microglia in the chick embryo spinal cord: Implications in the regulation of motoneuronal survival and death. *Journal of Neuroscience Research* 87, 2447–2466. doi:10.1002/jnr.22084
- Doblado, L. R., Martínez-Ramos, C., Pradas, M. M. (2021). Biomaterials for Neural Tissue Engineering. *Frontiers in Nanotechnology*, 3. doi:10.3389/fnano.2021.643507
- Domínguez-Bajo, A., González-Mayorga, A., López-Dolado, E. et al. (2020). Graphene Oxide Microfibers Promote Regenerative Responses after Chronic Implantation in the Cervical Injured Spinal Cord. *ACS Biomaterials Science and Engineering* 6, 2401–2414. doi:10.1021/acsbiomaterials.0c00345
- Ferretti, P. and Whalley, K. (2008). Successful neural regeneration in amniotes: the developing chick spinal cord. *Cellular and Molecular Life Sciences* 65, 45–53. doi:10.1007/s00018-007-7430-2
- Führmann T., Anandakumaran, P. N., Shoichet, M. S. (2017). Combinatorial Therapies After Spinal Cord Injury: How Can Biomaterials Help? *Advanced Healthcare Materials* 6. doi:10.1002/adhm.201601130
- Galli, R., Sitoci-Ficici, K. H., Uckermann, O. et al. (2018). Label-free multiphoton microscopy reveals relevant tissue changes induced by alginate hydrogel implantation in rat spinal cord injury. *Scientific Reports* 8, 1–13. doi:10.1038/s41598-018-29140-z
- Guijarro-Belmar, A., Viskontas, M., Wei, Y. et al. (2019). Epac2 Elevation Reverses Inhibition by Chondroitin Sulfate Proteoglycans In Vitro and Transforms Postlesion Inhibitory Environment to Promote Axonal Outgrowth in an Ex Vivo Model of Spinal Cord Injury. *The Journal of Neuroscience : The Official Journal of the Society for Neuroscience* 39, 8330–8346. doi:10.1523/JNEUROSCI.0374-19.2019
- Hasan, S. J., Keirstead, H. S., Muir, G. D., & Steeves, J. D. (1993). Axonal regeneration contributes to repair of injured brainstem-spinal neurons in embryonic chick. *The Journal of Neuroscience* 13, 492–507. doi:10.1523/JNEUROSCI.13-02-00492.1993
- Himmels, P., Paredes, I., Adler, H. et al. (2017). Motor neurons control blood vessel patterning in the developing spinal cord. *Nature Communications* 8, 14583. doi:10.1038/ncomms14583
- Hurtado, A., Cregg, J. M., Wang, H. B. et al. (2011). Robust CNS regeneration after complete spinal cord transection using aligned poly-L-lactic acid microfibers. *Biomaterials* 32, 6068–6079. doi:10.1016/j.biomaterials.2011.05.006
- Kourgiantaki, A., Tzeranis, D. S., Karali, K. et al. (2020). Neural stem cell delivery via porous collagen scaffolds promotes neuronal differentiation and locomotion recovery in spinal cord injury. *Npj Regenerative Medicine* 5, 1–14. doi:10.1038/s41536-020-0097-0
- Lee, J. H., Shin, H., Shaker, M. R. et al. (2022). Production of human spinal-cord organoids recapitulating neural-tube morphogenesis. *Nat Biomed Eng* 6, 435-448. doi:10.1038/s41551-022-00868-4
- Mogas Barcons, A., Chari, D. M., & Adams, C. (2021). Enhancing the regenerative potential of stem cell-laden, clinical-grade implants through laminin engineering. *Materials Science and Engineering C* 123, 111931. doi:10.1016/j.msec.2021.111931
- Ogaki, A., Ikegaya, Y., Koyama, R. (2022) Replacement of Mouse Microglia With Human Induced Pluripotent Stem Cell (hiPSC)-Derived Microglia in Mouse Organotypic Slice Cultures. *Front Cell Neurosci* 16, 918442. doi:10.3389/fncel.2022.918442
- Sharma, A. L., Wang H., Zhang, Z. et al. (2022) HIV promotes neurocognitive impairment by damaging the hippocampal microvessels. *Mol Neurobiol* 59, 4966-4986. doi:10.1007/s12035-022-02890-8
- Shimizu, I., Oppenheim, R. W., O'Brien, M., & Shneiderman, a. (1990). Anatomical and functional recovery following spinal

- cord transection in the chick embryo. *J Neurobiol* 21, 918–937. doi:10.1002/neu.480210609
- Tubby, K. C., Norval, D., & Price, S. R. (2013). Chicken embryo spinal cord slice culture protocol. *Journal of Visualized Experiments* 73, 1–6. doi:10.3791/50295
- Walsh, C. M., Wychowanec, J. K., Costello, L. et al. (2023) An in vitro and ex vivo analysis of the potential of gelMA hydrogels as a therapeutic platform for preclinical spinal cord injury. *Advanced Healthcare Materials*, e2300951. doi:10.1002/adhm.202300951
- Weightman, A. P., Pickard, M. R., Yang, Y., & Chari, D. M. (2014). An in vitro spinal cord injury model to screen neuroregenerative materials. *Biomaterials* 35, 3756–3765. doi:10.1016/j.biomaterials.2014.01.022
- Whalley, K., O’Neill, P., & Ferretti, P. (2006). Changes in response to spinal cord injury with development: Vascularization, hemorrhage and apoptosis. *Neuroscience* 137, 821–832. doi:10.1016/j.neuroscience.2005.07.064
- Wu, G. H., Shi, H. J., Che, M. T. et al. (2018). Recovery of paralyzed limb motor function in canine with complete spinal cord injury following implantation of MSC-derived neural network tissue. *Biomaterials* 181, 15–34. doi:10.1016/j.biomaterials.2018.07.010
- Xue, W., Li, B., Liu, H. et al. (2022) Generation of dorsoventral human spinal cord organoids via functionalizing composite scaffold for drug testing. *iScience* 26, 105898. doi:10.1016/j.isci.2022.105898
- Yang, Z., Zhang, A., Duan, H. et al. (2015). NT3-chitosan elicits robust endogenous neurogenesis to enable functional recovery after spinal cord injury. *Proceedings of the National Academy of Sciences of the United States of America* 112, 13354–13359. doi:10.1073/pnas.1510194112
- Yang, C., Li, X., Li, S. et al. (2019) Organotypic slice culture based on in ovo electroporation for chicken embryonic central nervous system. *J Cell Mol Med* 23, 1813-1826. doi:10.1111/jcmm.14080

Data availability statement

Research data (raw images and quantification data) is available upon request from the corresponding author.

Conflict of interest

The authors have no conflicts of interest.

Acknowledgements

Work was supported by a Royal Society Research Grant (RGS\R2\180328; CFA) and the Faculty of Natural Sciences, Keele University.